Editors' Suggestion

Ultrafast X-Ray Scattering Measurements of Coherent Structural Dynamics on the Ground-State Potential Energy Surface of a Diplatinum Molecule

Kristoffer Haldrup,[1] Gianluca Levi,[2,3] Elisa Biasin,[1,4] Peter Vester,[1] Mads Goldschmidt Laursen,[1] Frederik Beyer,[1] Kasper Skov Kjær,[1,5,4] Tim Brandt van Driel,[1,6] Tobias Harlang,[1,5] Asmus O. Dohn,[2,7] Robert J. Hartsock,[4] Silke Nelson,[6] James M. Glownia,[6] Henrik T. Lemke,[6,8] Morten Christensen,[1] Kelly J. Gaffney,[4] Niels E. Henriksen,[2] Klaus B. Møller,[2] and Martin M. Nielsen[1]

[1]*Technical University of Denmark, Department of Physics, Fysikvej 307, DK-2800 Kongens Lyngby, Denmark*
[2]*Technical University of Denmark, Department of Chemistry, Kemitorvet 207, DK-2800 Kongens Lyngby, Denmark*
[3]*Current address: Science Institute of the University of Iceland, VR-III, 107 Reykjavík, Iceland*
[4]*PULSE Institute, SLAC National Accelerator Laboratory, Menlo Park, California 94025, USA*
[5]*Department of Chemical Physics, Lund University, Box 118, S-22100 Lund, Sweden*
[6]*LCLS, SLAC National Accelerator Laboratory, Menlo Park, California 94025, USA*
[7]*Science Institute of the University of Iceland, VR-III, 107 Reykjavík, Iceland*
[8]*SwissFEL, Paul Scherrer Institut, 5232 Villigen PSI, Switzerland*

(Received 16 July 2018; published 13 February 2019)

We report x-ray free electron laser experiments addressing ground-state structural dynamics of the diplatinum anion Pt_2POP_4 following photoexcitation. The structural dynamics are tracked with <100 fs time resolution by x-ray scattering, utilizing the anisotropic component to suppress contributions from the bulk solvent. The x-ray data exhibit a strong oscillatory component with period 0.28 ps and decay time 2.2 ps, and structural analysis of the difference signal directly shows this as arising from ground-state dynamics along the PtPt coordinate. These results are compared with multiscale Born-Oppenheimer molecular dynamics simulations and demonstrate how off-resonance excitation can be used to prepare a vibrationally cold excited-state population complemented by a structure-dependent depletion of the ground-state population which subsequently evolves in time, allowing direct tracking of ground-state structural dynamics.

DOI: 10.1103/PhysRevLett.122.063001

Optical lasers with femtosecond pulse lengths have enabled a host of studies of the excited-state kinetics and dynamics. With the arrival of x-ray and electron sources with pulse lengths in the subpicosecond regime, the bond-length and bond-angle dynamics of the photoexcited molecules can now be directly measured [1–3]. However, the majority of chemical reactions take place between molecular species in their electronic ground states and the energy landscape of ground-state molecules is therefore of fundamental interest. The dynamics of ground-state molecules have mainly been investigated through time-resolved optical methods based on preparing nonequilibrium, coherent vibrational states through combined absorption and Raman processes involving an excited-state potential surface. This is today a mature field spanning several methodologies, e.g., resonant impulsive stimulated Raman scattering (RISRS) and coherent anti-Stokes Raman scattering (CARS) [4–8]. These spectroscopy methods provide a powerful approach to characterizing vibrational eigenfrequencies for harmonic modes, but do not directly access bond lengths and angles. Similar limitations apply to the so-called *Lochfrass* or "*R*-dependent ionization" spectroscopies, where the ground state is selectively depleted as a function of some key structural parameter [9–12].

The reliance on indirect, albeit powerful, spectroscopic methods to probe the potential energy landscape of ground-state molecules has been due to a lack of structurally sensitive probes with the requisite time resolution. Here we show how hard x-ray free electron laser (XFEL) sources [13] now make it possible to directly map the structural dynamics of an ensemble of molecules as it evolves on the ground-state potential surface. Illustrating this approach, we investigate how the ground-state population of the much-studied diplatinum anion PtPOP $[Pt_2(P_2O_5H_2)_4]^{4-}$ (Fig. 1) [14–23] evolves following Pt-Pt distance-dependent photodepletion of the ground-state population.

Our structural analysis of the x-ray data is compared with multiscale Born-Oppenheimer molecular dynamics (BOMD) simulations, combining quantum mechanics with molecular mechanics (QM/MM) to calculate forces [51–53]. Following Fleming and co-workers [41], the simulations are used to model the dynamics of a ground-state nonequilibrium density created by the pump pulse through propagation of a so-called hole in the classical ground-state equilibrium distribution mirroring

at time zero the distribution promoted to the excited state. The ground-state dynamics predicted this way becomes increasingly accurate in the high temperature limit ($T \gg \Theta$, where $\Theta = h\nu/k_B$ is the vibrational temperature) as more vibrational levels of the ground state are initially populated (for PtPOP the ground-state vibrational temperature is 170 K giving a vibrational excitation fraction [54] of ≈0.6 at 300 K).

The photophysics of PtPOP have been studied for four decades [22] and it is well established that excitation in the absorption band centered at 370 nm promotes an electron from the antibonding $5d\sigma^*$ HOMO orbital to the bonding $6p\sigma$ LUMO orbital [14]. Excitation to the $p\sigma$ orbital, located between the two Pt atoms, leads to a shortening of the Pt-Pt equilibrium distance from $d^{gs}_{PtPt} = 2.9$–3.0 to $d^{es}_{PtPt} = 2.7$–2.8 Å, with the bond shortening being closely similar in both the singlet ($\tau_{S_1} = 10$–30 ps) and triplet ($\tau_{T_1} = 10$ μs) excited states [15–18,23]. Figure 1 shows the potential surfaces of the ground and S_1 excited state, the shape and positions of which determine the structural dynamics following photoexcitation. Excitation around $\lambda = 370$ nm leads to well-defined harmonic oscillations with period T^{es} close to 0.225 ps [19,21,23] as molecules near the bottom of the ground-state potential surface are promoted to S_1.

Low-temperature optical spectroscopy in the crystal phase [14] and Raman spectroscopy in solution [55,56] determined the ground-state potential to be also highly harmonic but slightly softer than the singlet- and triplet-state potentials with a Pt-Pt oscillation with period $T^{gs} = 0.285$ ps. Whereas much effort has been devoted towards investigating the energy dissipation mechanisms and structural dynamics of the excited-state structure(s) of PtPOP [53,57–59], no studies have directly addressed the ground-state dynamics. Here we utilize off-resonance excitation at 395 nm to selectively excite solute molecules near the excited-state equilibrium geometry, see Fig. 1.

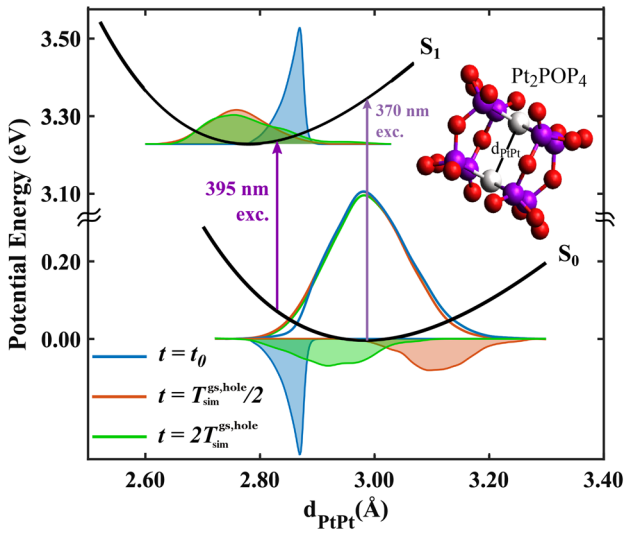

FIG. 1. Ground- and excited-state potential surfaces and QM/MM BOMD simulation of the structural dynamics following photoexcitation at 395 nm. The distribution of Pt-Pt distances is given by blue, red, and green lines, representing the time steps $t = 0$, $t = T^{gs,hole}_{sim}/2$, and $t = 2T^{gs,hole}_{sim}$. An animation of the time evolution can be found in the Supplemental Material [24].

To complement the experiments, the structural evolution following off-resonance excitation of PtPOP was also investigated via multiscale QM/MM BOMD simulations. Full descriptions of the methods are given in Refs. [52,53]. Briefly, PtPOP was modeled using DFT with the BLYP functional [37,38], and a representation of the Kohn-Sham (KS) orbitals in terms of tzp basis set for the Pt atoms and dzp for the rest of the atoms [36]. The TIP4P force field [60] was used for the surrounding solvent. The simulations were realized using the BOMD code and QM/MM interfacing scheme [52] implemented in ASE [32,33] and GPAW [34,35].

To model the off-resonance excitation process, the simulation procedure first established a large set of ground-state configurations. From these, a subset with sufficiently short Pt-Pt distances to allow excitation to the singlet excited state by a 395 nm (≈3.14 eV) photon was selected. Photoexcitation to the S_1 singlet state of PtPOP was modeled by starting 50 independent trajectories from this subset of ground-state configurations using the ΔSCF method [53,61]. The procedure thus established two sets of trajectories, representing propagation of a depleted ground-state ensemble and of an excited-state ensemble. Figure 1 shows the d_{PtPt} distributions following the excitation event. We note that the semiclassical picture used to predict the dynamics taking place in the ground state after interaction with a short pump pulse implicitly incorporates effects that are commonly thought of as originating from a combination of absorption and impulsive stimulated Raman scattering [41].

Laser-pump or x-ray probe experiments were conducted at the LCLS facility. The XFEL delivered < 50 fs 9.5 keV x-ray pulses at 120 Hz to the XPP experiment station [62], where the x-ray beam was focused to 30×30 μm^2. Laser excitation was by <50 fs 395(5) nm pulses, focused to a circular spot of <150 μm diameter and with a pulse energy of 3 μJ/pulse. The sample consisted of a 50 μm diameter free-flowing cylindrical jet of an 80 mM aqueous solution of PtPOP, with a flow speed sufficient to ensure full replenishment between pump and probe events. Scattered x rays were detected by the 2D CSPAD [63] detector placed ≈5 cm behind the sample, allowing a Q-space coverage up to $Q = 5$ Å^{-1}, with $Q = (4\pi/\lambda)\sin(2\theta/2)$, where 2θ is the scattering angle and λ is the x-ray wavelength (1.31 Å). Following detector corrections, background subtraction, and outlier rejection as previously described [64], 2D difference scattering images were constructed by subtracting laser-off images from laser-on images, where the laser had interacted with the sample at time t relative to the x-ray probe.

Designating the scattering patterns with and without the excitation laser interacting with the sample as "On" and "Off" the difference signal is

$$\Delta S(t) = S^{\mathrm{On}}(t) - S^{\mathrm{Off}}. \quad (1)$$

For the experiments and analysis described here, the individual difference scattering images were rebinned and subsequently averaged in 10 fs time bins according to the upstream timing tool [65] with approximately 150 images in each bin.

The contribution to the scattering patterns from the solute molecules is designated as either gs or es corresponding to ground- and excited-state molecules, the Off signal is the scattering from just the ground-state equilibrium distribution of structures, whereas the On signal arises from two contributions:

$$S^{\mathrm{Off}} = S^{\mathrm{gs,eq}};$$
$$S^{\mathrm{On}}(t) = \alpha S^{\mathrm{es}}(t) + [S^{\mathrm{gs,eq}} - \alpha S^{\mathrm{gs,hole}}(t)], \quad (2)$$

where α denotes the fraction of photoexcited PtPOP molecules in the probed sample volume at the given time delay. The term in the parentheses describes the population of ground-state molecules, of which the fraction α has been promoted to the excited state. The difference scattering signal is thus given by

$$\Delta S(t) = \alpha[S^{\mathrm{es}}(t) - S^{\mathrm{gs,hole}}(t)]. \quad (3)$$

As such, the acquired difference scattering signal arises from both the excited-state population as well as from the "hole" that the excitation pulse created in the ground state.

The 2D difference images as acquired are anisotropic, with the anisotropic contribution to the scattering arising from preferential excitation of molecules with the transition dipole moment aligned parallel with the polarization of the excitation laser pulse. When the subsequent structural changes have a specific orientation with respect to the transition dipole moment, then the resulting scattering patterns will necessarily be anisotropic. This is the case here, as the $d\sigma^* \rightarrow p\sigma$ absorption peak has a transition dipole moment aligned along the Pt-Pt axis along which the Pt nuclei contract following photoexcitation. The difference scattering signal from such a distribution of solute molecules is described by [66–68]

$$\Delta S(Q,t) = \Delta S_0(Q,t) + P_2[\cos(\theta_q)]\Delta S_2(Q,t); \quad (4)$$

here the geometry of the experiment is introduced through θ_q, the angle between the laser polarization axis and $\mathbf{Q}$, with P_2 being a second-order Legendre polynomium.

Assuming that the solute in each of the vibrational ensembles es and gs,hole can be represented by a single average structure, the isotropic ΔS_0 and anisotropic ΔS_2 parts of the solute contributions to the difference scattering signal are calculated from [68,69]

$$S_0(Q) = \sum_{i,j}^{N} f_i(Q) f_j(Q) \frac{\sin(Q r_{ij})}{Q r_{ij}};$$
$$S_2(Q) = -c_2 \sum_{i,j}^{N} f_i(Q) f_j(Q) P_2[\cos(\xi_{ij})] j_2(r_{ij}); \quad (5)$$

here we have suppressed the time dependence for clarity of presentation. In these expressions, r_{ij} is the length of the vector $\mathbf{r_{ij}}$ connecting atoms i and j and ξ_{ij} is the angle between $\mathbf{r_{ij}}$ and the transition dipole moment of the molecule. j_2 the second-order spherical Bessel function and f_i refers to the form factor of atom i in the molecule consisting of N atoms. The time evolution of the orientational distribution is described by the prefactor $c_2(t)$ [68].

For the structural analysis presented here, the isotropic $\Delta S_0(Q)$ and anisotropic $\Delta S_2(Q)$ contributions to the difference signal were separated [67,68]. The analysis presented below is focused on $\Delta S_2(Q,t)$, as this part of the full difference signal arises only from structural changes with a well-defined relationship to the excitation laser polarization axis and as such contains no contribution from the (isotropic) heating of the bulk solvent. The analysis of $\Delta S_0(Q,t)$ is shown in the Supplemental Material [24], with key results reported in Figs. 3 and 4.

Figure 2 shows $\Delta S_2(Q,t)$, where following photoexcitation at $t = 0$ a positive feature appears at low Q, indicative of a decrease in the average Pt-Pt distance in the probed sample volume. In the following picoseconds, the difference signal oscillates in intensity with little change in signal shape. Applying a singular value decomposition to $\Delta S_2(Q,t)$ (Supplemental Material [24]), the inset shows the Fourier transform of the time dependence of the

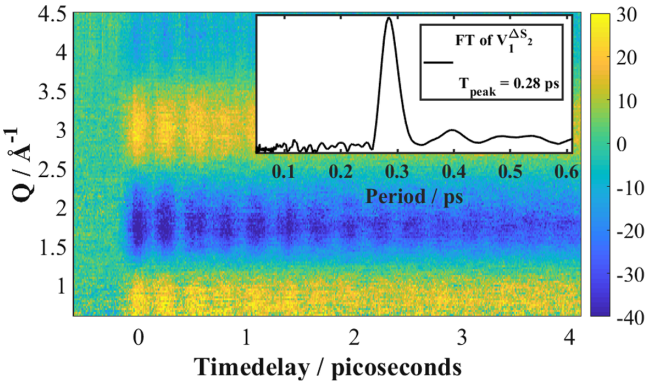

FIG. 2. $\Delta S_2(Q,t)$ with the color scale given in ‰ units of total signal. The inset shows the Fourier transform of the first right-singular vector of an SVD analysis $|\mathcal{F}(V_1^{\Delta S_2})|$. A sharp peak at the 0.28 ps ground-state period of PtPOP is observed.

acquired signal as described by the first right-singular vector of the difference signal, $|\mathcal{F}(V_1^{\Delta S_2})|$. From this, we find that structural dynamics of the photoexcited sample gives rise to a difference scattering signal exhibiting a pronounced oscillatory behavior with a period T_{peak} close to 0.285 ps. This value is in very good agreement with the ground-state frequency of the Pt-Pt oscillations and significantly different from the $T^{\mathrm{es}} = 0.210$–0.225 ps period of the singlet and triplet excited states [14,19,21]. From time-domain Fourier transforms of ΔS_0 and ΔS_2 (Supplemental Material [24]), we estimate that contributions from excited-state dynamics ($T^{es}_{\mathrm{peak}} = 0.21$–$0.23$ ps) to the observed difference signals is at most around 10%. We ascribe this to two main factors: (i) off-resonance excitation, and (ii) within-pulse motion of the Pt nuclei smearing out the dynamics in the excited state more significantly than in the ground state. As such, photoexcitation at 395 nm preferentially excites the subpopulation of PtPOP molecules with short Pt-Pt distances, that is, near the potential energy minimum of the singlet excited state (Fig. 1). The photoexcited molecules therefore exhibit little or no coherent vibrational dynamics. Simultaneously, the ground-state population as characterized by the distribution of Pt-Pt distances is now no longer in equilibrium, as molecules with short Pt-Pt bond lengths have been preferentially excited. As the ensemble of molecules evolves, the ground-state population of molecules characterized at $t = 0$ by long Pt-Pt distances ($d_{\mathrm{PtPt}} \sim 3.1$ Å) will after $T^{\mathrm{gs}}/2$ have moved to short Pt-Pt distances, thus filling the hole at $d_{\mathrm{PtPt}} = 2.77$ Å, which consequently moves to long Pt-Pt distances. In the following picoseconds, the hole propagates on the ground-state potential surface, eventually broadening to reflect the equilibrium ground-state distribution of Pt-Pt distances.

The difference signal $\Delta S(Q,t)$ was analyzed by structural fitting, employing a model incorporating a Pt-Pt distance-dependent depletion of the ground-state population as described above.

Within this analysis framework [17,70], the excitation fraction and key structural parameters (here d_{PtPt}) are known to be strongly correlated [71]. To enable the robust determination of bond-length dynamics, the excitation fraction was first estimated by analyzing the difference signal at $t = 5$ ps where both the excited- and ground-state populations have reached their equilibrium distributions. The model applied in this step utilizes DFT-derived structures for the ground and excited state of PtPOP while maintaining the excitation fraction α as a free parameter. Obtaining a photoexcitation fraction $\alpha = 0.018(2)$, the second step of the structural analysis relies on locking this parameter in the analysis of the full data set. The difference signal modeling further assumes the excited-state population to have $d_{\mathrm{PtPt}} = 2.77$ Å for all time delays, while the ground-state distribution is assumed to be given by a combination of the ground-state equilibrium structure minus a hole characterized by a time-dependent Pt-Pt distance $d^{\mathrm{hole}}_{\mathrm{PtPt}}(t)$. The model with which the observed time-dependent difference scattering signal was fit is thus

$$\Delta S_2(Q,t) = \alpha\{S_2^{\mathrm{es}}(Q) - S_2^{\mathrm{gs,hole}}[Q, d^{\mathrm{hole}}_{\mathrm{PtPt}}(t)]\}, \quad (6)$$

with all structural dynamics parametrized through the position of the ground-state hole, $d^{\mathrm{hole}}_{\mathrm{PtPt}}(t)$ and with the scattering signals calculated through Eq. (5).

Figure 3 shows the fit at a representative time delay, $t = 0.25$ ps, and Fig. 4(a) shows the best-fit value for $d^{\mathrm{hole}}_{\mathrm{PtPt}}$ as a function of time delay t. $d^{\mathrm{hole}}_{\mathrm{PtPt}}$ is observed to move towards larger values immediately after excitation and then oscillates around the ground-state equilibrium distance in agreement with the discussion above. The time dependence is well described by an (IRF-broadened) exponentially damped sine function convoluted with a step function centered at $t = 0$. Fitting this function to $d^{\mathrm{hole}}_{\mathrm{PtPt}}(t)$ we find a period $T^{\mathrm{gs,hole}} = 0.283(1)$ ps and decay time $\tau^{\mathrm{gs,hole}} = 2.2(2)$ ps.

Figure 4(b) shows the corresponding results of our QM/MM BOMD simulations. From these, we obtain a period of $T^{\mathrm{gs,hole}}_{\mathrm{sim}} = 0.271$ ps, which agrees to within 5% with the experimental data. The decay of the oscillations takes place in $\tau^{\mathrm{gs,hole}}_{\mathrm{sim}} = 0.7$ ps, which is 3 times faster than observed experimentally. We tentatively ascribe this difference as arising from the simulations overestimating the anharmonicity of the Pt-Pt potential. This is supported by the observation that the period of the simulated oscillations changes by around 20 fs from the first oscillation to the last, while no change can be discerned from the analysis of the experimental data.

The period and decay time of the observed oscillations derived from the ΔS_2 analysis, $T^{\mathrm{gs,hole}} = 0.283(1)$ ps and $\tau^{\mathrm{gs,hole}} = 2.2(2)$ ps, are in very good agreement with optical studies of PtPOP in ethylene glycol and in

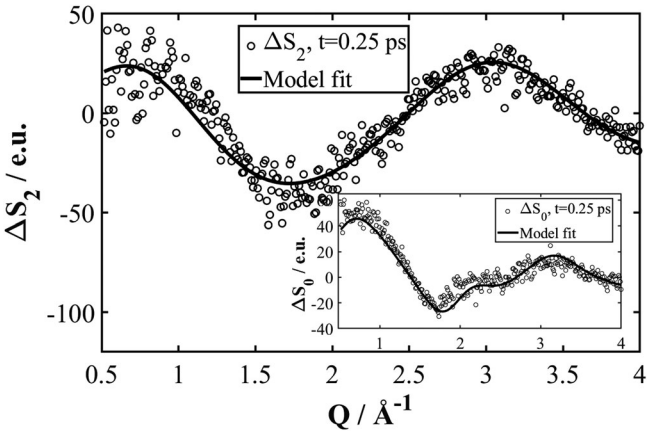

FIG. 3. ΔS_2 and model fit at $t = 0.25$ ps after photoexcitation. Inset shows the corresponding fit of ΔS_0 at the same time delay.

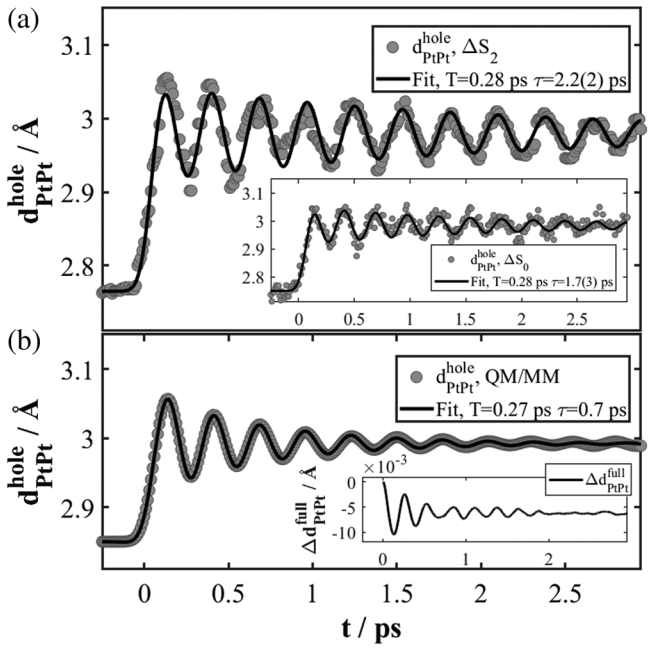

FIG. 4. (a) Time-dependent evolution of $d^{\mathrm{hole}}_{\mathrm{PtPt}}$ (gray circles). The dynamics have been fit (black line) with an IRF-broadened, exponentially damped sine function convoluted with a step function. Inset shows the ΔS_0 results. (b) Time-dependent position of the hole (gray circles) from the simulations fitted with the same function (black line) as the experimental results. Inset shows the average Pt-Pt distance for the entire simulated ensemble.

acetonitrile where $T^{\mathrm{gs}} = 0.281(3)$ and $\tau^{\mathrm{gs}} = 2.2(2)$ ps were found [19,23]. The slightly faster decay time observed in the ΔS_0 analysis [$\tau^{\mathrm{gs,hole}} = 1.7(3)$ ps] is likely spurious and arising from a small contribution from two-photon excitation of PtPOP to $\Delta S_0(Q,t)$ as discussed in the Supplemental Material [24].

The amplitude of the $d^{\mathrm{hole}}_{\mathrm{PtPt}}$ oscillation is 0.06(1) Å, which is somewhat shorter than inferred from optical data [19] but in full agreement with the simulation result shown in Fig. 4. The lower amplitude can thus be interpreted as due to the analysis tracking only the central position of the $d^{\mathrm{hole}}_{\mathrm{PtPt}}$ distribution which rapidly broadens (Fig. 1).

The results presented demonstrate the preparation of a vibrationally cold excited-state population and the evolution of a ground-state hole. Comparison with simulations allows direct and experimentally supported visualization of how the population distributions evolve on both the ground- and excited-state potential surfaces. Future experiments with better Q-space coverage will allow us to follow these dynamics in more detail, as recently discussed from a theoretical point of view [72] and experimentally realized for the $\mathrm{Fe(bpy)_3}$ system using XAFS [73]. A key feature of the present experiment is the controlled preparation of a vibrationally cold excited state and we suggest that further studies utilizing vibrationally cold excited states may shed light on the temperature-dependent and highly elusive [22] mechanism of the singlet-triplet transition in PtPOP.

In summary, excitation with ultrashort optical laser pulses in combination with SASE-based x-ray laser sources can be used to prepare and track well-defined populations on the ground- and excited-state potential surfaces of molecules in solution. By choosing off-resonance excitation, the excited population can be prepared in a vibrationally cold state, allowing tracking of the ground-state dynamics alone.

The DTU-affiliated authors gratefully acknowledge DANSCATT for supporting the beamtime efforts. M. M. N., M. G. L., E. B., A. O. D., and K. B. M. thank the Independent Research Fund Denmark for financial support under Grants No. DFF-4002-00272 and No. DFF-8021-00347B. A. O. D. thanks the Icelandic Research Fund (Grant No. 174244-051) and the Villum Foundation for financial support. K. J. G. acknowledges support from the AMOS program within the Chemical Sciences, Geosciences and Biosciences Division of the Office of Basic Energy Sciences, Office of Science, U.S. Department of Energy. Use of the Linac Coherent Light Source (LCLS), SLAC National Accelerator Laboratory, is supported by the U.S. Department of Energy, Office of Science, Office of Basic Energy Sciences under Contract No. DE-AC02-76SF00515.

[1] T. Elsaesser, Introduction: Ultrafast processes in chemistry, Chem. Rev. **117**, 10621 (2017).
[2] M. Chergui and E. Collet, Photoinduced structural dynamics of molecular systems mapped by time-resolved X-ray methods, Chem. Rev. **117**, 11025 (2017).
[3] E. Collet and M. Cammarata, Disentangling ultrafast electronic and structural dynamics with X-ray lasers, Chem. Eur. J. **24**, 15696 (2018).
[4] U. Banin, A. Bartana, S. Ruhman, and R. Kosloff, Impulsive excitation of coherent vibrational motion ground state surface dynamics induced by intense short pulses, J. Chem. Phys. **101**, 8461 (1994).
[5] E. Gershgoren, J. Vala, R. Kosloff, and S. Ruhman, Impulsive control of ground surface dynamics of I-3(-) in solution, J. Phys. Chem. A **105**, 5081 (2001).
[6] A. M. Zheltikov, Coherent anti-Stokes Raman scattering: From proof-of-the-principle experiments to femtosecond CARS and higher order wave-mixing generalizations, J. Raman Spectrosc. **31**, 653 (2000).
[7] R. W. Hartsock, W. Zhang, M. G. Hill, B. Sabat, and K. J. Gaffney, Characterizing the deformational isomers of bimetallic $\mathrm{Ir_2(dimen)_4^{2+}}$ (dimen = 1, 8-diisocyano-*p*-menthane) with vibrational wavepacket dynamics, J. Phys. Chem. A **115**, 2920 (2011).
[8] R. R. Frontiera and R. A. Mathies, Femtosecond stimulated Raman spectroscopy, Laser Photonics Rev. **5**, 102 (2011).
[9] T. Ergler, B. Feuerstein, A. Rudenko, K. Zrost, C. D. Schroeter, R. Moshammer, and J. Ullrich, Quantum-Phase Resolved Mapping of Ground-State Vibrational D-2 Wave

Packets via Selective Depletion in Intense Laser Pulses, Phys. Rev. Lett. **97** (2006).
[10] E. Goll, G. Wunner, and A. Saenz, Formation of Ground-State Vibrational Wave Packets in Intense Ultrashort Laser Pulses, Phys. Rev. Lett. **97** (2006).
[11] L. Fang and G. N. Gibson, Strong-Field Induced Vibrational Coherence in the Ground Electronic State of Hot I(2), Phys. Rev. Lett. **100** (2008).
[12] J. Foerster, E. Plesiat, A. Magana, and A. Saenz, Imaging of the umbrella motion and tunneling in ammonia molecules by strong-field ionization, Phys. Rev. A **94** (2016).
[13] C. Bostedt, S. Boutet, D. M. Fritz, Z. Huang, H. J. Lee, H. T. Lemke, A. Robert, W. F. Schlotter, J. J. Turner, and G. J. Williams, Linac coherent light source: The first five years, Rev. Mod. Phys. **88** (2016).
[14] S. F. Rice and H. B. Gray, Electronic absorption and emission spectra of binuclear platinum(II) complexes—characterization of the lowest singlet and triplet excited states of $Pt_2(H_2P_2O_5)_4^{4-}$, J. Am. Chem. Soc. **105**, 4571 (1983).
[15] C. D. Kim, S. Pillet, G. Wu, W. K. Fullagar, and P. Coppens, Excited-state structure by time-resolved X-ray diffraction, Acta Crystallogr. Sect. A **58**, 133 (2002).
[16] N. Yasuda, M. Kanazawa, H. Uekusa, and Y. Ohashi, Excited-state structure of a platinum complex by X-ray analysis, Chem. Lett. **31**, 1132 (2002).
[17] M. Christensen, K. Haldrup, K. Bechgaard, R. Feidenhans'l, Q. Kong, M. Cammarata, M. L. Russo, M. Wulff, N. Harrit, and M. M. Nielsen, Time-resolved X-ray scattering of an electronically excited state in solution. Structure of the (3)A(2u) state of tetrakis-mu-pyrophosphitodiplatinate(II), J. Am. Chem. Soc. **131**, 502 (2009).
[18] R. M. van der Veen, C. J. Milne, A. El Nahhas, F. A. Lima, V.-T. Pham, J. Best, J. A. Weinstein, C. N. Borca, R. Abela, C. Bressler, and M. Chergui, Structural determination of a photochemically active diplatinum molecule by time-resolved EXAFS spectroscopy, Angew. Chem., Int. Ed. Engl. **48**, 2711 (2009).
[19] R. M. van der Veen, A. Cannizzo, F. van Mourik, A. Vlcek, Jr., and M. Chergui, Vibrational relaxation and intersystem crossing of binuclear metal complexes in solution, J. Am. Chem. Soc. **133**, 305 (2011).
[20] M.-O. Winghart, J.-P. Yang, M. Vonderach, A.-N. Unterreiner, D.-L. Huang, L.-S. Wang, S. Kruppa, C. Riehn, and M. M. Kappes, Time-resolved photoelectron spectroscopy of a dinuclear Pt(II) complex: Tunneling autodetachment from both singlet and triplet excited states of a molecular dianion, J. Chem. Phys. **144**, 054305 (2016).
[21] R. Monni, G. Aubck, D. Kinschel, K. M. Aziz-Lange, H. B. Gray, A. Vlek, and M. Chergui, Conservation of vibrational coherence in ultrafast electronic relaxation: The case of diplatinum complexes in solution, Chem. Phys. Lett. **683**, 112 (2017).
[22] H. B. Gray, S. Zalis, and A. Vlcek, Electronic structures and photophysics of d(8)-d(8) complexes, Coord. Chem. Rev. **345**, 297 (2017).
[23] R. Monni, G. Capano, G. Auböck, H. B. Gray, A. Vlček, I. Tavernelli, and M. Chergui, Vibrational coherence transfer in the ultrafast intersystem crossing of a diplatinum complex in solution, Proc. Natl. Acad. Sci. U.S.A. **115**, E6396 (2018).
[24] See Supplemental Material at http://link.aps.org/supplemental/10.1103/PhysRevLett.122.063001 for a description of sample synthesis, data reduction, time series and residual analysis, ΔS_0 analysis results and details of the QM/MM BOMD simulations, which includes Refs. [25–50].
[25] E. Biasin *et al.*, Femtosecond X-Ray Scattering Study of Ultrafast Photoinduced Structural Dynamics in Solvated $[Co(terpy)_2]^{2+}$, Phys. Rev. Lett. **117** (2016).
[26] C. M. Che, L. G. Butler, P. J. Grunthaner, and H. B. Gray, Chemistry and spectroscopy of binuclear diplatinum complexes, Inorg. Chem. **24**, 4662 (1985).
[27] K. S. Kjær, T. B. van Driel, J. Kehres, K. Haldrup, D. Khakhulin, K. Bechgaard, M. Cammarata, M. Wulff, T. J. Sorensen, and M. M. Nielsen, Introducing a standard method for experimental determination of the solvent response in laser pump, X-ray probe time-resolved wide-angle X-ray scattering experiments on systems in solution, Phys. Chem. Chem. Phys. **15**, 15003 (2013).
[28] K. Haldrup *et al.*, Observing solvation dynamics with simultaneous femtosecond X-ray emission spectroscopy and X-ray scattering, J. Phys. Chem. B **120**, 1158 (2016).
[29] J. R. Peterson and K. Kalyanasundaram, Energy-transfer and electron-transfer processes of the lowest triplet excited-state of tetrakis(diphosphito)diplatinate(II), J. Phys. Chem. **89**, 2486 (1985).
[30] D. Leshchev, T. C. B. Harlang, L. A. Fredin, D. Khakhulin, Y. Liu, E. Biasin, M. G. Laursen, G. E. Newby, K. Haldrup, M. M. Nielsen, K. Warnmark, V. Sundstrom, P. Persson, K. S. Kjaer, and M. Wulff, Tracking the picosecond deactivation dynamics of a photoexcited iron carbene complex by time-resolved X-ray scattering, Chem. Sci. **9**, 405 (2018).
[31] A. E. Stiegman, S. F. Rice, H. B. Gray, and V. M. Miskowski, Electronic spectroscopy of diplatinum complexes—excited states of $Pt_2(P_2O_5H_2)_4^{4-}$, Inorg. Chem. **26**, 1112 (1987).
[32] S. R. Bahn and K. W. Jacobsen, An object-oriented scripting interface to a legacy electronic structure code, Comput. Sci. Eng. **4**, 56 (2002).
[33] A. H. Larsen *et al.*, The atomic simulation environmenta python library for working with atoms, J. Phys. Condens. Matter **29**, 273002 (2017).
[34] J. J. Mortensen, L. B. Hansen, and K. W. Jacobsen, Real-space grid implementation of the projector augmented wave method, Phys. Rev. B **71**, 035109 (2005).
[35] J. Enkovaara *et al.*, Electronic structure calculations with gpaw: A real-space implementation of the projector augmented-wave method, J. Phys. Condens. Matter **22**, 253202 (2010).
[36] A. H. Larsen, M. Vanin, J. J. Mortensen, K. S. Thygesen, and K. W. Jacobsen, Localized atomic basis set in the projector augmented wave method, Phys. Rev. B **80**, 195112 (2009).
[37] A. D. Becke, Density-functional exchange-energy approximation with correct asymptotic behavior, Phys. Rev. A **38**, 3098 (1988).
[38] C. Lee, W. Yang, and R. G. Parr, Development of the Colle-Salvetti correlation-energy formula into a functional of the electron density, Phys. Rev. B **37**, 785 (1988).

[39] G. Levi, Photoinduced molecular dynamics in solution, Ph. D. thesis, Technical University of Denmark, 2018.

[40] W. L. Jorgensen, J. Chandrasekhar, J. D. Madura, R. W. Impey, and M. L. Klein, Comparison of simple potential functions for simulating liquid water, J. Chem. Phys. **79**, 926 (1983).

[41] D. M. Jonas, S. E. Bradforth, S. A. Passino, and G. R. Fleming, Femtosecond wavepacket spectroscopy—influence of temperature, wavelength and pulse duration, J. Phys. Chem. **99**, 2594 (1995).

[42] A. K. Rappe, C. J. Casewit, K. S. Colwell, W. A. Goddard III, and W. M. Skiff, Uff, a full periodic table force field for molecular mechanics and molecular dynamics simulations, J. Am. Chem. Soc. **114**, 10024 (1992).

[43] H. C. Andersen, Rattle: A "velocity" version of the shake algorithm for molecular dynamics calculations, J. Comput. Phys. **52**, 24 (1983).

[44] J. Petersen, N. E. Henriksen, and K. B. Møller, Validity of the Bersohn-Zewail model beyond justification, Chem. Phys. Lett. **539–540**, 234 (2012).

[45] K. B. Møller, R. Rey, and J. T. Hynes, Hydrogen bond dynamics in water and ultrafast infrared spectroscopy: A theoretical study, J. Phys. Chem. A **108**, 1275 (2004).

[46] V. A. Ermoshin and V. Engel, Femtosecond pump-probe fluorescence signals from classical trajectories: Comparison with wave-packet calculations, Eu. Phys. J. D **15**, 413 (2001).

[47] Z. Li, J.-Y. Fang, and C. C. Martens, Simulation of ultrafast dynamics and pump-probe spectroscopy using classical trajectories, J. Chem. Phys. **104**, 6919 (1996).

[48] E. H. Van Kleef and I. Powis, Anisotropy in the preparation of symmetric top excited states. I. One-photon electric dipole excitation, Mol. Phys. **96**, 757 (1999).

[49] R. J. Maurer and K. Reuter, Assessing computationally efficient isomerization dynamics: ΔSCF density-functional theory study of azobenzene molecular switching, J. Chem. Phys. **135**, 224303 (2011).

[50] B. Himmetoglu, A. Marchenko, I. Dabo, and M. Cococcioni, Role of electronic localization in the phosphorescence of iridium sensitizing dyes, J. Chem. Phys. **137**, 154309 (2012).

[51] A. O. Dohn, E. Ö. Jonsson, K. S. Kjær, T. B. van Driel, M. M. Nielsen, K. W. Jacobsen, N. E. Henriksen, and K. B. Møller, Direct dynamics studies of a binuclear metal complex in solution: The interplay between vibrational relaxation, coherence, and solvent effects, J. Phys. Chem. Lett. **5**, 2414 (2014).

[52] A. O. Dohn, Elvar Ö. Jonsson, G. Levi, J. J. Mortensen, O. Lopez-Acevedo, K. S. Thygesen, K. W. Jacobsen, J. Ulstrup, N. E. Henriksen, K. B. Møller, and H. Jonsson, Grid-based projector augmented wave (gpaw) implementation of quantum mechanics/molecular mechanics (qm/mm) electrostatic embedding and application to a solvated diplatinum complex, J. Chem. Theory Comput. **13**, 6010 (2017).

[53] G. Levi, M. Papai, N. E. Henriksen, A. O. Dohn, and K. B. Møller, Solution structure and ultrafast vibrational relaxation of the PtPOP complex revealed by delta SCF-QM/MM direct dynamics simulations, J. Phys. Chem. C **122**, 7100 (2018).

[54] D. A. McQuarrie, *Statistical Mechanics* (Harper & Row, New York, 1975).

[55] C. M. Che, F. H. Herbstein, W. P. Schaeffer, R. E. Marsh, and H. B. Gray, Binuclear platinum diphosphite complexes—crystal-structures of $K_4[Pt_2(POP)_4Br] - 3H_2O$, a new linear-chain semiconductor, and $K_4[Pt_2(POP)_4Cl_2] - 2H_2O$, J. Am. Chem. Soc. **105**, 4604 (1983).

[56] K. H. Leung, D. L. Phillips, C. M. Che, and V. M. Miskowski, Resonance Raman intensity analysis investigation of metal-metal bonded transitions: An examination of the $_1A^{2u}¡ - {}_1A^{1g}(5d\sigma * - ¢6p\ \sigma)$ transition of $Pt_2(H_2P_2O_5)_4{}^{4-}$, J. Raman Spectrosc. **30**, 987 (1999).

[57] A. C. Durrell, G. E. Keller, Y.-C. Lam, J. Sykora, A. Vlcek, Jr., and H. B. Gray, Structural control of (1)A(2u)-to-(3)A (2u) intersystem crossing in diplatinum (II,II) complexes, J. Am. Chem. Soc. **134**, 14201 (2012).

[58] S. Zalis, Y.-C. Lam, H. B. Gray, and A. Vlcek, Spin-orbit TDDFT electronic structure of diplatinum (II,II) complexes, Inorg. Chem. **54**, 3491 (2015).

[59] Y. C. Lam, H. B. Gray, and J. R. Winkler, Intersystem crossing in diplatinum complexes, J. Phys. Chem. A **120**, 7671 (2016).

[60] W. L. Jorgensen, Quantum and statistical mechanical studies of liquids. 10. transferable intermolecular potential functions for water, alcohols, and ethers. application to liquid water, J. Am. Chem. Soc. **103**, 335 (1981).

[61] J. Gavnholt, T. Olsen, M. Engelund, and J. Schiotz, Delta self-consistent field method to obtain potential energy surfaces of excited molecules on surfaces, Phys. Rev. B **78** (2008).

[62] M. Chollet, R. Alonso-Mori, M. Cammarata, D. Damiani, J. Defever, J. T. Delor, Y. Feng, J. M. Glownia, J. B. Langton, S. Nelson, K. Ramsey, A. Robert, M. Sikorski, S. Song, D. Stefanescu, V. Srinivasan, D. Zhu, H. T. Lemke, and D. M. Fritz, The X-ray pump-probe instrument at the linac coherent light source, J. Synchrotron Radiat. **22**, 503 (2015).

[63] H. T. Philipp, M. Hromalik, M. Tate, L. Koerner, and S. M. Gruner, Pixel array detector for X-ray free electron laser experiments, Nucl. Instrum. Methods Phys. Res., Sect. A **649**, 67 (2011); 16th Pan-American Conference on Synchrotron Radiation Instrumentation (SRI2010), Chicago, IL, 2010.

[64] T. B. van Driel, K. S. Kjaer, E. Biasin, K. Haldrup, H. T. Lemke, and M. M. Nielsen, Disentangling detector data in XFEL studies of temporally resolved solution state chemistry, Faraday Discuss. **177**, 443 (2015).

[65] M. Harmand, R. Coffee, M. R. Bionta, M. Chollet, D. French, D. Zhu, D. M. Fritz, H. T. Lemke, N. Medvedev, B. Ziaja, S. Toleikis, and M. Cammarata, Achieving few-femtosecond time sorting at hard x-ray free-electron lasers, Nat. Photonics **7**, 215 (2013).

[66] J. S. Baskin and A. H. Zewail, Oriented ensembles in ultrafast electron diffraction, Chem. Phys. Chem. **7**, 1562 (2006).

[67] U. Lorenz, K. B. Møller, and N. E. Henriksen, On the interpretation of time-resolved anisotropic diffraction patterns, New J. Phys. **12**, 113022 (2010).

[68] E. Biasin, T. B. van Driel, G. Levi, M. G. Laursen, A. O. Dohn, A. Moltke, P. Vester, F. B. K. Hansen, K. S. Kjaer, T. Harlang, R. Hartsock, M. Christensen, K. J. Gaffney, N. E. Henriksen, K. B. Møller, K. Haldrup, and M. M. Nielsen, Anisotropy enhanced X-ray scattering from

solvated transition metal complexes, J. Synchrotron Radiat. **25**, 306 (2018).

[69] A. O. Dohn, E. Biasin, K. Haldrup, M. M. Nielsen, N. E. Henriksen, and K. B. Møller, On the calculation of X-ray scattering signals from pairwise radial distribution functions, J. Phys. B **49**, 244010 (2016).

[70] K. Haldrup, T. Harlang, M. Christensen, A. Dohn, T. B. van Driel, K. S. Kjaer, N. Harrit, J. Vibenholt, L. Guerin, M. Wulff, and M. M. Nielsen, Bond Shortening (1.4 angstrom) in the singlet and triplet excited states of $[Ir_2(dimen)_4]^{2+}$ in solution determined by time-resolved X-ray scattering, Inorg. Chem. **50**, 9329 (2011).

[71] K. Haldrup, M. Christensen, and M. M. Nielsen, Analysis of time-resolved X-ray scattering data from solution-state systems, Acta Crystallogr. Sect. A **66**, 261 (2010).

[72] A. Kirrander and P. M. Weber, Fundamental limits on spatial resolution in ultrafast X-ray diffraction, Appl. Sci. **7**, 534 (2017).

[73] H. T. Lemke, K. S. Kjaer, R. Hartsock, T. B. van Driel, M. Chollet, J. M. Glownia, S. Song, D. Zhu, E. Pace, S. F. Matar, M. M. Nielsen, M. Benfatto, K. J. Gaffney, E. Collet, and M. Cammarata, Coherent structural trapping through wave packet dispersion during photoinduced spin state switching, Nat. Commun. **8** (2017).